An r-adaptive, high-order discontinuous Galerkin method for flows with attached shocks

Matthew J. Zahr*
University of Notre Dame, Notre Dame, IN, 46556, U.S.A.

Per-Olof Persson†
University of California, Berkeley, Berkeley, CA 94720-3840, U.S.A.

This work extends the method developed in [1, 2] that uses a high-order discontinuous Galerkin discretization and optimization-based r-adaptivity to track discontinuous solutions of conservation laws with the underlying mesh and provide high-order accurate approximations without additional stabilization techniques, e.g., limiting or artificial viscosity, to problems with shocks attached to curved boundaries. Central to the framework is an optimization problem whose solution is a shock-aligned mesh and the corresponding DG approximation to the flow; in this sense, the framework is an implicit tracking method, which distinguishes it from methods that aim to explicitly mesh the shock surface. The optimization problem is solved using a sequential quadratic programming method that simultaneously converges the mesh and DG solution, which is critical to avoids nonlinear stability issues that would come from computing a DG solution on a unconverged (non-aligned) mesh. In the case of a shock attached to a curved boundary, the mesh coordinates are parametrized in terms of a reduced set of degrees of freedom and a mapping that ensures boundary nodes always conform to the appropriate boundary. We use the proposed method to solve for the inviscid, transonic flow around a NACA0012 airfoil. The framework generates a mesh that successfully tracks the attached shock and provides an accurate flow approximation on a relatively coarse mesh.

I. Introduction

High-order methods, such as the discontinuous Galerkin (DG) method [3, 4], are widely believed to be superior to traditional low-order schemes for simulation of turbulent flow problems. However, in the presence of shocks and other discontinuities, the lack of nonlinear stability proves to be a fundamental problem. Many solutions have been proposed, but new advances are still required to make these new schemes sufficiently robust and competitive for real-world problems.

Most of the techniques for addressing shocks are based on so-called *shock capturing*, that is, the numerical discretization somehow incorporates the discontinuities independently of the computational grid. One simple method is to use a sensor that identifies the mesh elements that contain shocks, and reduce their polynomial degrees [5, 6]. For the DG method, this essentially leads to a standard cell-centered finite volume scheme locally, which is well-known to handle shocks robustly. Related more sophisticated approaches include limiting, such as the weighted essentially non-oscillatory (WENO) schemes [7–9]. For high-order methods, artificial viscosity has also proven to be highly competitive, since it can smoothly resolve the jumps in the solution without introducing additional discontinuities between the elements [10]. The main problem with all these approaches is that they reduce to first order accuracy in the affected elements, which translates into a globally first order accurate scheme. This can be remedied by using local mesh refinement around the shock (h-adaptivity) [11], although the anisotropic elements that are required for efficiency are difficult to generate, and it usually generates excessively fine elements around the shock.

An alternative approach is *shock tracking* or *shock fitting*, where the computational mesh is moved such that their faces are aligned with the discontinuities in the solution [12–23]. This is very natural in the setting of a DG method, since the numerical scheme already incorporates jumps between the elements, and the approximate Riemann solvers employed on the element faces handle the discontinuities correctly. However, it is a difficult meshing problem since it essentially requires generating a fitted mesh to the (unknown) shock surface. Also, in the early approaches to shock

*Assistant Professor, Department of Aerospace and Mechanical Engineering, 300B Cushing Hall, Notre Dame, IN, 46556, AIAA Member. Email: mzahr@nd.edu

†Professor, Department of Mathematics, University of California, Berkeley, Berkeley, CA, AIAA Member. Email: persson@berkeley.edu.

fitting, it was applied to low-order schemes where the relative advantage over shock capturing is smaller than for high-order methods. Because of this, shock tracking is largely not used in practical CFD today.

In [1], we proposed a shock tracking approach for high-order DG schemes, based on an optimization problem whose solution is a shock-aligned mesh and the solution of the true DG discretization on this mesh. This leads to an implicit approach to tracking, rather than explicitly trying to mesh the shock surfaces. The method is truly high-order accurate, since the solution is smooth within each element, and very accurate solutions were obtained on coarse meshes. Further improvements in [2] increased the robustness of the approach. The key features of the method include an r-adaptive PDE-constrained optimization formulation, a solver that simultaneously converges the DG solution and the mesh to their optimal values and avoids nonlinear stability issues, as well as practical details such as mesh operations to remove skewed elements and initialization of the solution from the $p = 0$ DG solution. A related approach in [24, 25] uses a DG-like discretization with unconventional numerical fluxes and Rankine–Hugoniot conditions that are enforced in a minimum-residual sense.

In this work, we provide an overview of the method and apply it to the transonic flow over an airfoil. Since the shock is attached, this requires sliding nodes along the curved boundaries and re-parametrization of the optimization problem to incorporate the boundary constraints. We achieve this by introducing mappings, whose Jacobians are derived analytically and used in the optimization solver. We apply the method on the standard test case of transonic flow around a NACA0012 airfoil, and demonstrate that we can accurately represent the shock using very coarse mesh elements.

II. Governing equations and high-order discontinuous Galerkin discretization

Consider a general system of M inviscid conservation laws, defined on the physical domain $\Omega \subset \mathbb{R}^d$,

$$\begin{aligned} \nabla \cdot F(U) &= 0 && \text{in } \Omega \\ F(U) \cdot n &= q(U, n) && \text{on } \partial\Omega, \end{aligned} \tag{1}$$

where $U : \Omega \to \mathbb{R}^M$ is the solution of the system of conservation laws, $F : \mathbb{R}^M \to \mathbb{R}^{M\times d}$ is the physical flux, $n : \partial\Omega \to \mathbb{R}^d$ is the outward unit normal, $q : \mathbb{R}^M \times \mathbb{R}^d \to \mathbb{R}^M$ is the value of the flux in the normal direction on the boundary (boundary condition), and $\nabla := (\partial_{x_1}, \ldots, \partial_{x_d})$ is the gradient operator in the physical domain such that $\nabla w(x) = \begin{bmatrix} \partial_{x_1} w(x) & \cdots & \partial_{x_d} w(x) \end{bmatrix} \in \mathbb{R}^{N\times d}$ for any N vector-valued function w over Ω ($w(x) \in \mathbb{R}^N$ for $x \in \Omega$). The formulation of the conservation law in (1) is sufficiently general to encapsulate steady conservation laws in d-dimensional spatial domain or time-dependent conservation laws in a $(d-1)$-dimensional domain, i.e., a d-dimensional space-time domain. In general, the solution $U(x)$ may contain discontinuities, in which case, the conservation law (1) holds away from the discontinuities and the Rankine-Hugoniot conditions [26] holds at discontinuities.

It is convenient to explicitly treat deformations to the domain of the conservation law Ω by transforming to a fixed reference domain $\Omega_0 \subset \mathbb{R}^d$. Suppose the physical domain can be taken as the result of a diffeomorphism applied to a reference domain

$$\Omega = \mathcal{G}(\Omega_0), \tag{2}$$

where $\Omega_0 \subset \mathbb{R}^d$ is a fixed reference domain and $\mathcal{G} : \mathbb{R}^d \to \mathbb{R}^d$ is the diffeomorphism defining the domain mapping. The conservation law on the physical domain Ω is transformed to a conservation law on the reference domain

$$\begin{aligned} \nabla_X \cdot F_X(U_X, \mathcal{G}) &= 0 && \text{in } \Omega_0 \\ F_X(U_X, \mathcal{G}) \cdot N &= q_X(U_X, \mathcal{G}, N) && \text{on } \partial\Omega_0, \end{aligned} \tag{3}$$

where $\nabla_X := (\partial_{X_1}, \ldots, \partial_{X_d})$ denotes spatial derivatives with respect to the reference domain Ω_0 with coordinates X, $U_X : \Omega_0 \to \mathbb{R}^M$ is the mapped state vector we define as

$$U_X = U \circ \mathcal{G}, \tag{4}$$

$F_X(U_X, \mathcal{G}) \in \mathbb{R}^{M\times d}$ is the transformed flux function, and $q_X(U_X, \mathcal{G}, N) \in \mathbb{R}^M$ is the transformed boundary condition. The unit normal in the reference and physical domain are related by

$$n = \frac{gG^{-T}N}{\|gG^{-T}N\|}, \tag{5}$$

where $G(X) = \frac{\partial}{\partial X}\mathcal{G}(X)$ is the deformation gradient of the domain mapping and $g(X) = \det G(X)$ is the Jacobian. The transformed flux and boundary condition are

$$F_X(U_X, \mathcal{G}) = gF(U)G^{-T}, \qquad q_X(U_X, \mathcal{G}, N) = \left\|gG^{-T}N\right\| q(U, n); \tag{6}$$

for details of the derivation, see [2].

We use a standard nodal discontinuous Galerkin method [3, 4] to discretize the transformed conservation law (3). Let $\mathcal{E}_{h,q}$ represent a discretization of the reference domain Ω_0 into non-overlapping, potentially curved, computational elements, where h is a mesh element size parameter and q is the polynomial order associated with the curved elements. The DG weak formulation of the transformed conservation law is

$$\int_{\partial K} \psi_X^+ \cdot \mathcal{H}_X(U_X^+, U_X^-, N, \mathcal{G})\, dS - \int_K F(U_X, \mathcal{G}) : \nabla_X \psi_X \, dV = 0, \tag{7}$$

where $\mathcal{H}_X(U_X^+, U_X^-, N, \mathcal{G})$ is the numerical flux function, U_X^+ denotes the interior trace of U_X, U_X^- denotes the exterior trace of U_X if ∂K is an interior face, i.e., $\partial K \cap \partial\Omega_0 = \emptyset$, otherwise U_X^- is taken from a boundary condition.

To establish the algebraic form of (7), we introduce a nodal bases over each element for the solution, test function, and domain deformation. Taking the test and trial spaces to be piecewise polynomial spaces of equal degree p and the domain deformation to lie in the same piecewise polynomial space as the mesh (degree q), we obtain the discrete DG residual

$$\boldsymbol{r}(\boldsymbol{u}, \boldsymbol{x}) = \boldsymbol{0}, \tag{8}$$

where $\boldsymbol{u} \in \mathbb{R}^{N_{\boldsymbol{u}}}$ are the assembled coefficients of the solution U_X and $\boldsymbol{x} \in \mathbb{R}^{N_{\boldsymbol{x}}}$ are the assembled coefficients of the domain deformation $\mathcal{G}$ (coordinates of the mesh in the physical domain). We also introduce an *enriched* discrete residual $\boldsymbol{R}(\boldsymbol{u}, \boldsymbol{x})$, defined as the discrete DG residual corresponding to a trial space of degree p, test space of degree $p+1$, and deformation space of degree q. Both $\boldsymbol{r}(\boldsymbol{u}, \boldsymbol{x})$ and $\boldsymbol{R}(\boldsymbol{u}, \boldsymbol{x})$ will be used to define the tracking optimization problem.

III. Shock tracking framework via optimization-based r-refinement

In this section, we introduce the main contribution of this work: an r-adaptivity framework that recasts the discrete conservation law (8) as a PDE-constrained optimization problem over the discrete solution and mesh that aims to align features in the solution basis with features in the solution itself. In the present setting, this amounts to aligning element faces with discontinuities. The method builds upon our previous work [1, 2], where we demonstrated that high-order methods are capable of approximating discontinuous solutions of PDEs using extremely coarse discretizations provided the discontinuities are tracked.

A. PDE-constrained optimization formulation

Following our work in [1, 2], we formulate the problem of tracking discontinuities as a PDE-constrained optimization problem over the PDE state and coordinates of the mesh nodes that minimizes some objective function $f : \mathbb{R}^{N_{\boldsymbol{u}}} \times \mathbb{R}^{N_{\boldsymbol{x}}} \to \mathbb{R}$ while enforcing the DG discretization of the conservation law

$$\begin{aligned} &\underset{\boldsymbol{u}\in\mathbb{R}^{N_{\boldsymbol{u}}}, \boldsymbol{x}\in\mathbb{R}^{N_{\boldsymbol{x}}}}{\text{minimize}} && f(\boldsymbol{u}, \boldsymbol{x}) \\ &\text{subject to} && \boldsymbol{r}(\boldsymbol{u}, \boldsymbol{x}) = \boldsymbol{0}. \end{aligned} \tag{9}$$

The objective function is constructed such that the solution of the PDE-constrained optimization problem is a mesh that aligns with discontinuities in the solution. The optimization-based tracking method directly inherits the benefits of standard DG methods, i.e., high-order accuracy and conservation, due to the constraint that exactly enforces the DG discretization. The optimization formulation in (9) will provide nonlinear stability without using limiting or artificial viscosity if all discontinuities are successfully tracked.

In [2], we proposed an objective function that penalizes a measure of the DG solution error using the enriched residual. Since a piecewise polynomial solution on an aligned mesh will have much lower error than on a non-aligned mesh, error-based indicators tend to promote alignment of the mesh with discontinuities. We use the norm of the DG residual corresponding to an enriched *test space*, i.e.,

$$f(\boldsymbol{u}, \boldsymbol{x}) \coloneqq \frac{1}{2}\boldsymbol{R}(\boldsymbol{u}, \boldsymbol{x})^T \boldsymbol{R}(\boldsymbol{u}, \boldsymbol{x}), \tag{10}$$

where we enrich the test space using polynomials of one degree higher than the trial space, a term often found in adjoint-based error estimation [27].

B. Enforcement of boundary constraints

To maintain a boundary-conforming mesh, the coordinates of all mesh nodes cannot be allowed to move freely; rather, we must add boundary constraints to ensure nodes *slide* along the domain boundaries. To this end, we write the mesh node coordinates as the result of a mapping $\chi : \mathbb{R}^{N_{\phi}} \to \mathbb{R}^{N_{x}}$ from the unconstrained degrees of freedom $\boldsymbol{\phi} \in \mathbb{R}^{N_{\phi}}$ that incorporates all boundary constraints

$$\boldsymbol{x} = \chi(\boldsymbol{\phi}), \tag{11}$$

where the specific form of the mapping depends on the domain under consideration. This constraint is incorporated into the optimization problem (9) as:

$$\begin{aligned} \underset{\boldsymbol{u}\in\mathbb{R}^{N_{\boldsymbol{u}}},\boldsymbol{\phi}\in\mathbb{R}^{N_{\boldsymbol{\phi}}}}{\text{minimize}} \quad & f(\boldsymbol{u}, \chi(\boldsymbol{\phi})) \\ \text{subject to} \quad & \boldsymbol{r}(\boldsymbol{u}, \chi(\boldsymbol{\phi})) = \boldsymbol{0}. \end{aligned} \tag{12}$$

For example, consider the NACA0012 airfoil and associated flow domain (Figure 1) from Section IV. We consider four separate surfaces that nodes are permitted to slide along: the upper/lower halves of the farfield boundary and the upper/lower surface of the airfoil. The upper and lower halves of the farfield boundary can be written as functions $y_{cu} : (-1.5, 2.5) \to \mathbb{R}$ and $y_{cl} : (-1.5, 2.5) \to \mathbb{R}$, respectively, as

$$y_{cu}(x) = \sqrt{4 - (x - 0.5)^2}, \qquad y_{cl}(x) = -\sqrt{4 - (x - 0.5)^2}. \tag{13}$$

The upper and lower surfaces of the airfoil can be written as functions $y_{au} : (0, 1) \to \mathbb{R}$ and $y_{al} : (0, 1) \to \mathbb{R}$, respectively, as

$$\begin{aligned} y_{au}(x) &= 0.6\left(0.2960\sqrt{x} - 0.126x - 0.3516x^2 + 0.2843x^3 - 0.1036x^4\right) \\ y_{al}(x) &= -0.6\left(0.2960\sqrt{x} - 0.126x - 0.3516x^2 + 0.2843x^3 - 0.1036x^4\right). \end{aligned} \tag{14}$$

We ensure the reference mesh is constructed such that a node that lies precisely at the junction between any of these four surfaces and we do not allow them to move. For this geometry, this corresponds to nodes at $(-1.5, 0)$, $(2.5, 0)$, $(0, 0)$, $(0, 1)$.

Without loss of generality, we assume the degrees of freedom defining the mesh coordinates $\boldsymbol{x}$ are arranged as follows

$$\boldsymbol{x} = (\boldsymbol{X}_i, \boldsymbol{Y}_i, \boldsymbol{X}_{cu}, \boldsymbol{Y}_{cu}, \boldsymbol{X}_{cl}, \boldsymbol{Y}_{cl}, \boldsymbol{X}_{au}, \boldsymbol{Y}_{au}, \boldsymbol{X}_{al}, \boldsymbol{Y}_{al}, \boldsymbol{X}_f, \boldsymbol{Y}_f), \tag{15}$$

where $\boldsymbol{X}_i$, $\boldsymbol{Y}_i$ are the x- and y-coordinates of the interior nodes, i.e., not on a boundary, $\boldsymbol{X}_f$, $\boldsymbol{Y}_f$ are the x- and y-coordinates of the fixed nodes, $\boldsymbol{X}_{cu}$, $\boldsymbol{Y}_{cu}$ are the x- and y-coordinates of the nodes on the upper half of the circle, $\boldsymbol{X}_{cl}$, $\boldsymbol{Y}_{cl}$ are the x- and y-coordinates of the nodes on the lower half of the circle, $\boldsymbol{X}_{au}$, $\boldsymbol{Y}_{au}$ are the x- and y-coordinates of the nodes on the upper surface of the airfoil, $\boldsymbol{X}_{al}$, $\boldsymbol{Y}_{al}$ are the x- and y-coordinates of the nodes on the lower surface of the airfoil. Then we define the free degrees of freedom as

$$\boldsymbol{\phi} = (\boldsymbol{X}_i, \boldsymbol{Y}_i, \boldsymbol{X}_{cu}, \boldsymbol{X}_{cl}, \boldsymbol{X}_{au}, \boldsymbol{X}_{al}) \tag{16}$$

and the mapping from unconstrained degrees of freedom to the mesh coordinates as

$$\chi(\boldsymbol{\phi}; \boldsymbol{X}_f, \boldsymbol{Y}_f) = \left(\boldsymbol{X}_i, \boldsymbol{Y}_i, \boldsymbol{X}_{cu}, y_{cu}(\boldsymbol{X}_{cu}), \boldsymbol{X}_{cl}, y_{cl}(\boldsymbol{X}_{cl}), \boldsymbol{X}_{au}, y_{au}(\boldsymbol{X}_{au}), \boldsymbol{X}_{al}, y_{al}(\boldsymbol{X}_{al}), \boldsymbol{X}_f, \boldsymbol{Y}_f\right). \tag{17}$$

The mapping Jacobian is easily determined from (17) as

$$\frac{\partial \chi}{\partial \boldsymbol{\phi}}(\boldsymbol{\phi}) = \begin{bmatrix} \boldsymbol{I} & & & & & \\ & \boldsymbol{I} & & & & \\ & & \boldsymbol{I} & & & \\ & & y'_{cu}(\boldsymbol{X}_{cu}) & & & \\ & & & \boldsymbol{I} & & \\ & & & y'_{cl}(\boldsymbol{X}_{cl}) & & \\ & & & & \boldsymbol{I} & \\ & & & & y'_{au}(\boldsymbol{X}_{au}) & \\ & & & & & \boldsymbol{I} \\ & & & & & y'_{al}(\boldsymbol{X}_{al}) \\ \boldsymbol{0} & \boldsymbol{0} & \boldsymbol{0} & \boldsymbol{0} & \boldsymbol{0} & \boldsymbol{0} \\ \boldsymbol{0} & \boldsymbol{0} & \boldsymbol{0} & \boldsymbol{0} & \boldsymbol{0} & \boldsymbol{0} \end{bmatrix}, \tag{18}$$

which is needed to compute the derivatives of the objective function and constraint in (12) as

$$\frac{\partial f}{\partial \boldsymbol{\phi}}(\boldsymbol{u}, \chi(\boldsymbol{\phi})) = \frac{\partial f}{\partial \boldsymbol{x}}(\boldsymbol{u}, \chi(\boldsymbol{\phi}))\frac{\partial \chi}{\partial \boldsymbol{\phi}}(\boldsymbol{\phi}), \qquad \frac{\partial \boldsymbol{r}}{\partial \boldsymbol{\phi}}(\boldsymbol{u}, \chi(\boldsymbol{\phi})) = \frac{\partial \boldsymbol{r}}{\partial \boldsymbol{x}}(\boldsymbol{u}, \chi(\boldsymbol{\phi}))\frac{\partial \chi}{\partial \boldsymbol{\phi}}(\boldsymbol{\phi}) \tag{19}$$

that are required by the full-space optimization solver discussed in the next section.

C. Full-space optimization solver

To solve the boundary-constrained optimization problem in (12), we apply the sequential quadratic programming method with Levenberg-Marquardt Hessian approximation and globalization with a linesearch based on a ℓ_1 merit function introduced in [2]. Instead of using the identity matrix to regularize the Hessian approximation, the stiffness matrix of a continuous Galerkin finite element discretization of Poisson's equation [24] with piecewise constant coefficients inversely proportional to the volume of each element in the reference domain [2]. The regularization parameter is adaptively chosen using the algorithm introduced in [2] and the optimization iterations stop when the first-order optimality conditions of (12) are satisfied up to a tolerance (10^{-10} for the constraint and 10^{-6} for the other optimality conditions). The DG solution ($\boldsymbol{u}$) is initialized with the $p = 0$ DG solution of the governing equations on the reference mesh [2]. To ensure elements do not become unacceptably skewed, we remove elements via edge collapses [25] once the volume of the element drops below 20% of its original volume.

IV. Numerical experiment: Transonic flow over NACA0012 airfoil

The Euler equations govern the steady flow of an inviscid, compressible fluid through a domain $\Omega \subset \mathbb{R}^d$

$$(\rho v_j)_{,j} = 0, \quad (\rho v_i v_j + p\delta_{ij})_{,j} = 0, \quad (\rho H v_i)_{,j} = 0 \quad \text{in } \Omega \tag{20}$$

where $\rho : \Omega \times (0, T) \to \mathbb{R}_+$ is the density of the fluid, $v_i : \Omega \times (0, T) \to \mathbb{R}$ for $i = 1, \ldots, d$ is the velocity of the fluid in the ith coordinate direction, and $E : \Omega \times (0, T) \to \mathbb{R}_+$ is the total energy of the fluid. The enthalpy of the fluid $H : \Omega \times (0, T) \to \mathbb{R}_+$ is defined as

$$\rho H = \rho E + P, \tag{21}$$

where $P : \Omega \times (0, T) \to \mathbb{R}_+$ is the pressure. For a calorically ideal fluid, the pressure and energy are related via the ideal gas law

$$P = (\gamma - 1)\left(\rho E - \frac{\rho v_i v_i}{2}\right) \tag{22}$$

and the speed of sound is $c = \sqrt{\gamma P/\rho}$. The density, velocity, and energy are combined into a vector of conservative variables as

$$U = \begin{bmatrix} \rho \\ \rho v \\ \rho E \end{bmatrix} \tag{23}$$

and the Euler equations take the form of an inviscid conservation law (1).

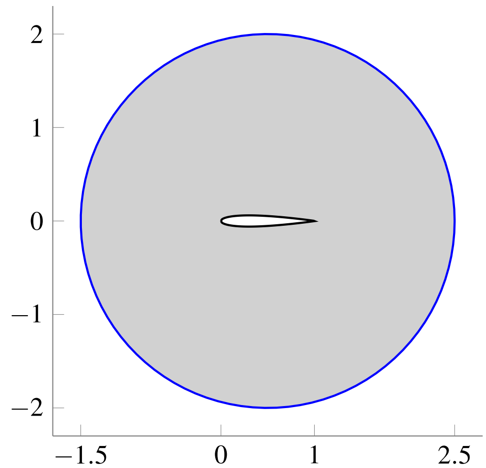

Fig. 1 Geometry and boundary conditions for the NACA0012 transonic flow test case. Boundary conditions: slip wall (——) and farfield (characteristic) conditions with $\rho_\infty = 1.4$, $v_\infty = (0.8\cos\theta, 0.8\sin\theta)$ ($M_\infty = 0.8$ and angle of attack $\theta = 1.5°$), and $p_\infty = 1$ (——).

We apply the DG discretization from Section II to the Euler equations and use Roe's flux [28] with Harten's entropy fix [15] as the numerical flux function. Using a mesh with only 809 elements, we apply the tracking framework to approximate the transonic flow. Figure 2 shows the solution using $p = q = 1$ and $p = q = 2$ elements. The solution is clearly underresolved with linear, straight-sided elements and well-resolved with quadratic elements.

V. Conclusion

In this work, we demonstrated the optimization-based, r-adaptive shock tracking framework for the high-order approximation of transonic, inviscid flow over an airfoil (shock attached to a curved surface). The key features of the shock tracking framework are: (1) a high-order DG discretization of the flow equations on a deformable domain and (2) *implicit* tracking via optimization-based r-adaptivity, i.e., the shock-aligned mesh and corresponding flow solution are the solution of an optimization problem constrained by the DG discretization. Nonlinear stability is achieved by simultaneously solving for the aligned mesh and corresponding flow solution, thereby avoiding solving the DG equations on a non-aligned mesh, which is known to be unstable in the presence of shocks. On a relatively coarse, unstructured mesh with no knowledge of the shock location, the tracking framework found a high-order mesh that tracks the curved shock and the corresponding DG solution.

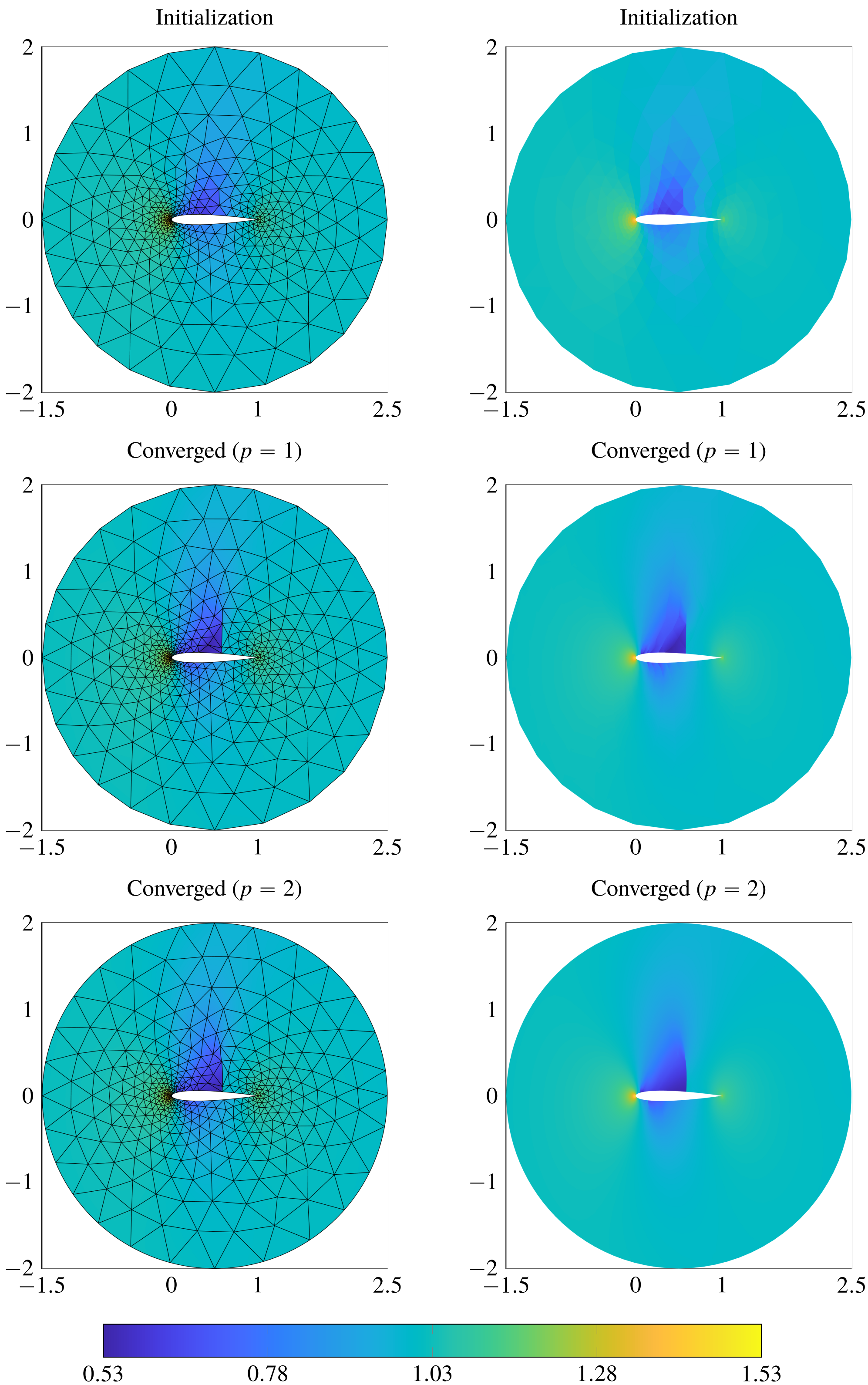

Fig. 2 Solution of the transonic flow past a NACA0012 airfoil at $M_\infty = 0.8$ and angle of attack $\theta = 1.5°$. On a relatively coarse mesh with 809 elements, the tracking framework successfully locates the discontinuity and provides an accurate solution.

References

[1] Zahr, M. J., and Persson, P.-O., "An optimization-based approach for high-order accurate discretization of conservation laws with discontinuous solutions," *Journal of Computational Physics*, Vol. 365, 2018, pp. 105 – 134. doi:https://doi.org/10.1016/j.jcp.2018.03.029, URL `http://www.sciencedirect.com/science/article/pii/S002199911830189X`.

[2] Zahr, M. J., Shi, A., and Persson, P.-O., "Shock tracking using an optimization-based, r-adaptive, high-order discontinuous Galerkin method," *in review*, 2019.

[3] Cockburn, B., and Shu, C.-W., "Runge-Kutta discontinuous Galerkin methods for convection-dominated problems," *J. Sci. Comput.*, Vol. 16, No. 3, 2001, pp. 173–261.

[4] Hesthaven, J., and Warburton, T., *Nodal Discontinuous Galerkin Methods: Algorithms, Analysis, and Applications*, Springer Science & Business Media, 2007.

[5] Baumann, C. E., and Oden, J. T., "A discontinuous *hp* finite element method for the Euler and Navier-Stokes equations," *Int. J. Numer. Methods Fluids*, Vol. 31, No. 1, 1999, pp. 79–95. Tenth International Conference on Finite Elements in Fluids (Tucson, AZ, 1998).

[6] Burbeau, A., Sagaut, P., and Bruneau, C.-H., "A problem-independent limiter for high-order Runge-Kutta discontinuous Galerkin methods," *Journal of Computational Physics*, Vol. 169, No. 1, 2001, pp. 111–150.

[7] Harten, A., Engquist, B., Osher, S., and Chakravarthy, S. R., "Uniformly high-order accurate essentially nonoscillatory schemes. III," *Journal of Computational Physics*, Vol. 71, No. 2, 1987, pp. 231–303. URL `https://doi.org/10.1016/0021-9991(87)90031-3`.

[8] Liu, X.-D., Osher, S., and Chan, T., "Weighted essentially non-oscillatory schemes," *Journal of Computational Physics*, Vol. 115, No. 1, 1994, pp. 200–212. URL `https://doi.org/10.1006/jcph.1994.1187`.

[9] Jiang, G.-S., and Shu, C.-W., "Efficient implementation of weighted ENO schemes," *Journal of Computational Physics*, Vol. 126, No. 1, 1996, pp. 202–228. URL `https://doi.org/10.1006/jcph.1996.0130`.

[10] Persson, P.-O., and Peraire, J., "Sub-Cell Shock Capturing for Discontinuous Galerkin Methods," *44th AIAA Aerospace Sciences Meeting and Exhibit, Reno, Nevada*, 2006. AIAA-2006-0112.

[11] Dervieux, A., Leservoisier, D., George, P.-L., and Coudière, Y., "About theoretical and practical impact of mesh adaptation on approximation of functions and PDE solutions," *International Journal for Numerical Methods in Fluids*, Vol. 43, No. 5, 2003, pp. 507–516. ECCOMAS Computational Fluid Dynamics Conference, Part I (Swansea, 2001).

[12] Shubin, G., Stephens, A., and Glaz, H., "Steady shock tracking and Newton's method applied to one-dimensional duct flow," *Journal of Computational Physics*, Vol. 39, No. 2, 1981, pp. 364–374.

[13] Shubin, G., Stephens, A., Glaz, H., Wardlaw, A., and Hackerman, L., "Steady shock tracking, Newton's method, and the supersonic blunt body problem," *SIAM Journal on Scientific and Statistical Computing*, Vol. 3, No. 2, 1982, pp. 127–144.

[14] Bell, J., Shubin, G., and Solomon, J., "Fully implicit shock tracking," *Journal of Computational Physics*, Vol. 48, No. 2, 1982, pp. 223–245.

[15] Harten, A., and Hyman, J. M., "Self adjusting grid methods for one-dimensional hyperbolic conservation laws," *Journal of computational Physics*, Vol. 50, No. 2, 1983, pp. 235–269.

[16] Van Rosendale, J., "Floating Shock Fitting via Lagrangian Adaptive Meshes," Tech. Rep. ICASE Report No. 94-89, Institute for Computer Applications in Science and Engineering, 1994.

[17] Trepanier, J.-Y., Paraschivoiu, M., Reggio, M., and Camarero, R., "A Conservative Shock Fitting Method on Unstructured Grids," *Journal of Computational Physics*, Vol. 126, No. 2, 1996, pp. 421 – 433. doi:https://doi.org/10.1006/jcph.1996.0147, URL `http://www.sciencedirect.com/science/article/pii/S0021999196901473`.

[18] Zhong, X., "High-order finite-difference schemes for numerical simulation of hypersonic boundary-layer transition," *Journal of Computational Physics*, Vol. 144, No. 2, 1998, pp. 662–709. URL `https://doi.org/10.1006/jcph.1998.6010`.

[19] Taghaddosi, F., Habashi, W., Guevremont, G., and Ait-Ali-Yahia, D., "An adaptive least-squares method for the compressible Euler equations," *International Journal for Numerical Methods in Fluids*, Vol. 31, No. 7, 1999, pp. 1121–1139.

[20] Baines, M., Leary, S., and Hubbard, M., "Multidimensional Least Squares Fluctuation Distribution Schemes with Adaptive Mesh Movement for Steady Hyperbolic Equations," *SIAM Journal on Scientific Computing*, Vol. 23, No. 5, 2002, pp. 1485–1502. doi:10.1137/S1064827500370202, URL https://doi.org/10.1137/S1064827500370202.

[21] Roe, P., and Nishikawa, H., "Adaptive grid generation by minimizing residuals," *International Journal for Numerical Methods in Fluids*, Vol. 40, No. 1-2, 2002, pp. 121–136.

[22] Glimm, J., Li, X., Liu, Y., Xu, Z., and Zhao, N., "Conservative Front Tracking with Improved Accuracy," *SIAM Journal on Numerical Analysis*, Vol. 41, No. 5, 2003, pp. 1926–1947. doi:10.1137/S0036142901388627, URL https://doi.org/10.1137/S0036142901388627.

[23] Palaniappan, J., Miller, S. T., and Haber, R. B., "Sub-cell shock capturing and spacetime discontinuity tracking for nonlinear conservation laws," *International Journal for Numerical Methods in Fluids*, Vol. 57, No. 9, 2008, pp. 1115–1135.

[24] Corrigan, A., Kercher, A., Kessler, D., and Wood-Thomas, D., "Convergence of the Moving Discontinuous Galerkin Method with Interface Condition Enforcement in the Presence of an Attached Curved Shock," *AIAA Aviation 2019 Forum*, 2019, p. 3207.

[25] Corrigan, A., Kercher, A., and Kessler, D., "A moving discontinuous Galerkin finite element method for flows with interfaces," *International Journal for Numerical Methods in Fluids*, Vol. 89, No. 9, 2019, pp. 362–406.

[26] Majda, A., *Compressible fluid flow and systems of conservation laws in several space variables*, Vol. 53, Springer Science & Business Media, 2012.

[27] Fidkowski, K., and Darmofal, D., "Review of output-based error estimation and mesh adaptation in computational fluid dynamics," *AIAA Journal*, Vol. 49, No. 4, 2011, pp. 673–694.

[28] Roe, P. L., "Approximate Riemann solvers, parameter vectors, and difference schemes," *Journal of Computational Physics*, Vol. 43, No. 2, 1981, pp. 357–372.